



1 Technical Note: Multiple wavelet coherence for untangling scale-specific  
2 and localized multivariate relationships in geosciences

3 Wei Hu<sup>2,3</sup> and Bing Cheng Si<sup>1,3</sup>

4 *<sup>1</sup>College of Hydraulic and Architectural Engineering, Northwest A&F University, Yangling*  
5 *712100, China*

6 *<sup>2</sup>New Zealand Institute for Plant & Food Research Limited, Private Bag 4704, 8140 Christchurch,*  
7 *New Zealand*

8 *<sup>3</sup>University of Saskatchewan, Department of Soil Science, Saskatoon, SK S7N 5A8, Canada*

9 Correspondence to: Wei Hu (wei.hu@plantandfood.co.nz) and Bing Cheng Si (bing.si@usask.ca)

## 10 Abstract

11 The scale-specific and localized bivariate relationships in geosciences can be  
12 revealed using simple wavelet coherence. The objective of this study is to develop a  
13 multiple wavelet coherence method for examining scale-specific and localized  
14 multivariate relationships. Stationary and non-stationary artificial datasets, generated  
15 with the response variable as the summation of five predictor variables (cosine waves)  
16 with different scales, were used to test the new method. Comparisons were also  
17 conducted using existing multivariate methods including multiple spectral coherence  
18 and multivariate empirical mode decomposition (MEMD). Results show that multiple  
19 spectral coherence is unable to identify localized multivariate relationships and  
20 underestimates the scale-specific multivariate relationships for non-stationary  
21 processes. The MEMD method was able to separate all variables into components at



22 the same set of scales, revealing scale-specific relationships when combined with  
23 multiple correlation coefficients, but has the same weakness as multiple spectral  
24 coherence. However, multiple wavelet coherences are able to identify scale-specific  
25 and localized multivariate relationships, as they are close to 1 at multiple scales and  
26 locations corresponding to those of predictor variables. Therefore, multiple wavelet  
27 coherence outperforms other common multivariate methods. Multiple wavelet  
28 coherence was applied to a real dataset and revealed the optimal combination of  
29 factors for explaining temporal variation of free water evaporation at Changwu site in  
30 China at multiple scale-location domains. Matlab codes for multiple wavelet  
31 coherence are developed and provided in the supplement.

## 32 1. Introduction

33 Geoscience data such as topography, climate, and ocean waves usually present  
34 cyclic patterns, with high-frequency (small-scale) processes being superimposed on  
35 low-frequency (large-scale) processes (Si, 2008). More often than not, geoscience  
36 data is non-stationary, consisting of a variety of frequency regimes that may be  
37 localized in space or time (Torrence and Compo, 1998; Si and Zeleke, 2005; Graf et  
38 al., 2014). The wavelet method is a common tool for detecting multi-scale and  
39 localized features of non-stationary processes in geosciences. Simple wavelet  
40 coherency has been widely used for untangling scale-specific and localized  
41 relationships for non-stationary processes in areas including geophysics (Lakshmi et  
42 al., 2004; Müller et al., 2008), hydrology (Labat et al., 2005; Das and Mohanty, 2008;



43 Tang and Piechota, 2009; Carey et al., 2013; Graf et al., 2014), soil science (Si and  
44 Zeleke, 2005; Biswas and Si, 2011), meteorology (Torrence and Compo, 1998), and  
45 ecology (Polansky et al., 2010). This method, however, is limited to two variables.  
46 Processes in geosciences are usually complex and may be affected by more than two  
47 environmental factors. A method is needed for analyzing multivariate (>2 variables)  
48 and localized relationships at multiple scales.

49 Several methods have been used for characterizing multivariate relationships. For  
50 example, multiple spectral coherence (MSC) has been used to explore the  
51 scale-specific relationships between soil saturated hydraulic conductivity ( $K_s$ ) and  
52 multiple soil physical properties (Koopmans, 1974; Si, 2008), but requires a stationary  
53 data series which is rare in geosciences. Multivariate empirical mode decomposition  
54 (MEMD), a data-driven method, decomposes each variable into different components  
55 (intrinsic mode functions (IMFs)) with each IMF corresponding to a “common scale”  
56 inherent in multiple variables (Rehman and Mandic, 2010). The MEMD method is  
57 meritorious due to its ability to deal with both non-stationary and nonlinear systems.  
58 The combination of squared multiple correlation coefficient and MEMD ( $MCC_{memd}$ )  
59 has been used to explore the multivariate control of soil water content or saturated  
60 hydraulic conductivity at multiple scales (Hu and Si, 2013; She et al., 2013, 2015; Hu  
61 et al., 2014). However, the sum of variances from different components typically does  
62 not equal the total variance of the original series, which may result in misleading  
63  $MCC_{memd}$  results. In addition, in geosciences, multivariate relationships are most  
64 likely to change with time or space due to non-stationarity of the processes involved.



65 However, localized multivariate relationships are not available using any of the  
66 existing multivariate methods. Therefore, it is required to extend the wavelet  
67 coherence from two variables to multiple variables.

68 An attempt to extend wavelet coherence from two to three variables has been made  
69 by Mihanović et al. (2009). Their method was also applied later in the marine sciences  
70 (Ng and Chan, 2012a, b). Limitations arise when using three variable wavelet  
71 coherence: first, only two predictor variables are considered; second, the two  
72 predictor variables must be orthogonal. Otherwise, extremely high or low (spurious)  
73 coherence ( $\gg 1$  or  $< 0$ ) may be produced. This spuriousness is inconsistent with the  
74 definition of coherence and may limit the application of this method in geosciences,  
75 where environmental variables are usually cross-correlated. Therefore, a robust  
76 method for calculating MWC, which produces coherence in the closed interval of [0,  
77 1], is needed.

78 The objective of this paper is to develop an MWC that applies to cases where there  
79 are multiple environmental variables of which may be cross-correlated. This method  
80 is first tested with artificial datasets to demonstrate its advantages over existing  
81 multivariate methods. It is then applied to a temporal series of evaporation ( $E$ ) from  
82 free water surface and meteorological factors at Changwu site in Shaanxi, China.

## 83 **2. Theory**

84 Simple wavelet coherence can be understood as the traditional correlation  
85 coefficient localized in the scale-location domain (Grinsted et al., 2004). Just as



86 correlation coefficients can be extensions from two variables to multiple (>2)  
 87 variables, wavelet coherence between two variables may also be extended to multiple  
 88 variables. Similar to simple wavelet coherence, MWC is based on a series of auto-  
 89 and cross-wavelet power spectra at different scales and spatial (or temporal) locations  
 90 for the response variable and all predictor variables.

91 Following Koopman (1974), a matrix representation of the smoothed auto- and  
 92 cross-wavelet power spectra for multiple predictor variables  $X$  ( $X = \{X_1, X_2, \dots, X_q\}$ )  
 93 can be written as

$$94 \quad \vec{W}^{X,X}(s, \tau) = \begin{bmatrix} \vec{W}^{X_1, X_1}(s, \tau) & \vec{W}^{X_1, X_2}(s, \tau) & \dots & \vec{W}^{X_1, X_q}(s, \tau) \\ \vec{W}^{X_2, X_1}(s, \tau) & \vec{W}^{X_2, X_2}(s, \tau) & \dots & \vec{W}^{X_2, X_q}(s, \tau) \\ \vdots & \vdots & & \vdots \\ \vec{W}^{X_q, X_1}(s, \tau) & \vec{W}^{X_q, X_2}(s, \tau) & \dots & \vec{W}^{X_q, X_q}(s, \tau) \end{bmatrix}, \quad (1)$$

95 where  $\vec{W}^{X_i, X_j}(s, \tau)$  is the smoothed auto-wavelet power spectra (when  $i=j$ ) or  
 96 cross-wavelet power spectra (when  $i \neq j$ ) at scale  $s$  and spatial (or temporal) location  
 97  $\tau$  respectively. For the detailed calculation of smoothed auto- and cross-wavelet  
 98 power spectra, see Supplement, Sect. S1.

99 The matrix of smoothed cross wavelet power spectra between response variable  $Y$   
 100 and predictor variables  $X_i$  can be defined as

$$101 \quad \vec{W}^{Y,X}(s, \tau) = \left[ \vec{W}^{Y, X_1}(s, \tau) \quad \vec{W}^{Y, X_2}(s, \tau) \quad \dots \quad \vec{W}^{Y, X_q}(s, \tau) \right], \quad (2)$$

102 where  $\vec{W}^{Y, X_i}(s, \tau)$  is the smoothed cross-wavelet power spectra between  $Y$  and  $X_i$  at  
 103 scale  $s$  and spatial (or temporal) location  $\tau$ .

104 The smoothed wavelet power spectrum of response variable  $Y$  is  $\vec{W}^{Y,Y}(s, \tau)$ .

105 Following Koopmans (1974), the MWC at scale  $s$  and location  $\tau$ ,  $\rho_m^2(s, \tau)$ , can



106 be written as

$$107 \quad \rho_m^2(s, \tau) = \frac{\overline{W}^{Y,X}(s, \tau) \overline{W}^{X,X}(s, \tau)^{-1} \overline{W}^{Y,X}(s, \tau)}{\overline{W}^{Y,Y}(s, \tau)}. \quad (3)$$

108 When only one predictor variable (e.g.,  $XI$ ) is included in  $X$ , Eq. (3) is the equation

109 for simple wavelet coherence,  $\rho_s^2(s, \tau)$ , between two variables (Torrence and

110 Webster, 1999; Grinsted et al., 2004):

$$111 \quad \rho_s^2(s, \tau) = \frac{\overline{W}^{Y,XI}(s, \tau) \overline{W}^{Y,XI}(s, \tau)}{\overline{W}^{XI,XI}(s, \tau) \overline{W}^{Y,Y}(s, \tau)}. \quad (4)$$

112 Therefore, simple wavelet coherence is consistent with multiple wavelet coherence

113 if only one predictor variable is included. In addition, the wavelet phase between a

114 response variable ( $Y$ ) and a predictor variable ( $XI$ ) is

$$115 \quad \phi(s, \tau) = \tan^{-1}(\text{Im}(W^{Y,XI}(s, \tau)) / \text{Re}(W^{Y,XI}(s, \tau))), \quad (5)$$

116 where Im and Re denote the imaginary and real part of  $W^{Y,XI}(s, \tau)$  respectively.

117 Note that the phase information between a response variable  $Y$  and multiple predictor

118 variables  $X$  cannot be obtained.

119 Multiple wavelet coherence at the 95% confidence level is calculated using the

120 Monte Carlo method (Grinsted et al., 2004). Surrogate spatial series (i.e., red noise) of

121 all variables are generated with a Monte Carlo simulation based on their first-order

122 autocorrelation coefficient (AR1). The MWC at each scale and location is calculated

123 using the simulated spatial series. This is repeated an adequate number of times (e.g.,

124 1000) (Grinsted et al., 2004). At each scale, MWCs at all locations outside the cones

125 of influence from all simulations are ranked in ascending order. The value at the 95th



126 percentile represents the 95% confidence level for the MWC at that scale. The Matlab  
127 codes and user manual document for calculating MWC and significance level are  
128 provided in the Supplement (Sect. S2–S4).

### 129 **3. Data and analysis**

#### 130 **3.1 Artificial data for method test**

131 The method is tested using a stationary and non-stationary artificial dataset  
132 generated following Yan and Gao (2007). The response variable ( $y$  for the stationary  
133 case and  $z$  for the non-stationary case) encompasses five cosine waves ( $y_1$  to  $y_5$  for  
134 the stationary case and  $z_1$  to  $z_5$  for the non-stationary case) with different  
135 dimensionless scales (Fig. 1). For the stationary case,  $y_1 = \cos(2\pi x/4)$ ,  $y_2 = \cos(2\pi x/8)$ ,  
136  $y_3 = \cos(2\pi x/16)$ ,  $y_4 = \cos(2\pi x/32)$ , and  $y_5 = \cos(2\pi x/64)$ , where  $x = 0, 1, 2, \dots, 255$ .  
137 There is one regular cycle every 4, 8, 16, 32, and 64 locations, representing  
138 dimensionless scales of 4, 8, 16, 32, and 64 for  $y_1$ ,  $y_2$ ,  $y_3$ ,  $y_4$ , and  $y_5$  respectively  
139 (Fig. 1a). The regular cycles make each predictor and response series stationary. For  
140 the non-stationary case,  $z_1 = \cos(500\pi(x/1000)^{0.5})$ ,  $z_2 = \cos(250\pi(x/1000)^{0.5})$ ,  
141  $z_3 = \cos(125\pi(x/1000)^{0.5})$ ,  $z_4 = \cos(62.5\pi(x/1000)^{0.5})$ , and  $z_5 = \cos(31.25\pi(x/1000)^{0.5})$ ,  
142 where  $x = 0, 1, 2, \dots, 255$ . The equation with the square root of the location term  
143 results in the gradual change in frequency (scale), with the greatest dimensionless  
144 scales of 4, 8, 16, 32, and 64 at the right hand side for  $z_1$ ,  $z_2$ ,  $z_3$ ,  $z_4$ , and  $z_5$   
145 respectively (Fig. 1b). The average scales for these predictor variables are 3, 5, 9, 17,  
146 and 32 respectively. The location-varying scales make each predictor and response



147 variable non-stationary.

148 For both the stationary and non-stationary series, the variance of the response  
149 variable is 2.5. The predictor variables, each with a variance of 0.5, are orthogonal to  
150 each other, and contribute equally to the total variance of the response variable. The  
151 cosine-like artificial datasets mimic many time series such as seismic signals,  
152 turbulence, air temperature, precipitation, hydrologic fluxes, and the El  
153 Niño-Southern Oscillation. They also mimic spatial series such as ocean waves,  
154 seafloor bathymetry, land surface topography, and soil water content along a  
155 hummocky landscape in geosciences. Therefore, they are representative of a  
156 geoscience data series and are suitable for testing the new method.

157 Multiple wavelet coherence between the response variable  $y$  (or  $z$ ) and two ( $y_2$  and  
158  $y_4$ , or  $z_2$  and  $z_4$ ) or three ( $y_2$ ,  $y_3$ , and  $y_4$ , or  $z_2$ ,  $z_3$ , and  $z_4$ ) predictor variables were  
159 calculated. The advantage of the artificial data is that the known scale- and localized  
160 features for all variables, and the known relationships between the response and each  
161 predictor variable are exact. By definition, the coherence is 1 at scales corresponding  
162 to that of included predictor variables and 0 at other scales.

163 To demonstrate the advantages of MWC in dealing with abrupt changes (a type of  
164 transient and localized feature), the second half of the original series of  $y_2$  (or  $z_2$ ) or  
165  $y_4$  (or  $z_4$ ) is replaced by 0, and MWC between the response variable and new set of  
166 predictor variables is calculated. We anticipate that the coherence changes from 1 to 0  
167 at the location where the new predictor variable becomes 0.

168 Predictor variables may not be as regular as that shown in Fig. 1 and may also be





169 cross-correlated to one another. For these reasons, white noises with a mean of 0 and a  
170 standard deviation of 0.3, 1, and 4 are generated and added to predictor variables of  
171  $y_2$  (or  $z_2$ ) and  $y_4$  (or  $z_4$ ). The resulting noised series are termed weakly, moderately,  
172 and highly noised series respectively, and have a correlation coefficient of 0.9, 0.5,  
173 and 0.1 respectively, with their original predictor variable. Multiple wavelet  
174 coherences between the response variable and different predictor variables (original  
175 and noised series) are calculated to demonstrate the performance of MWC when  
176 noised or correlated predictor variables are involved. Only the non-stationary case  
177 will be demonstrated because the performances of MWC for stationary and  
178 non-stationary cases are similar.

179 The MWC is compared to the MSC (Koopmans, 1974; Si, 2008) and  $MCC_{memd}$  (Hu  
180 and Si, 2013). The MSC is calculated based on the calculated auto- and cross- power  
181 spectra using an equation similar to Eq. (3). The detailed introduction of this method  
182 can be found in Si (2008). For the calculation of  $MCC_{memd}$ , a set of response and  
183 predictor variables form a multivariate data series for MEMD. The MEMD is a data  
184 driven method and has the ability to align “common scales” present within  
185 multivariate data. Please refer to Rehman and Mandic (2010) and Hu and Si (2013)  
186 for the MEMD analysis and the website  
187 (<http://www.commsp.ee.ic.ac.uk/~mandic/research/emd.htm>) for the related Matlab  
188 codes. The original series of response and predictor variables can be decomposed into  
189 different components (IMFs) with different scales by the MEMD. For IMFs at the  
190 same scale, multiple stepwise regressions are conducted between response and



191 predictor variables, and the multiple correlation coefficients for each scale-specific  
192 IMF are calculated.

### 193 **3.2 Real data for application**

194 Daily evaporation ( $E$ ) from free water surfaces of E601 evaporation pan (pan  
195 diameter of 61.8 cm) and other meteorological factors (i.e., relative humidity, mean  
196 temperature, sun hours, and wind speed) were collected from January 1, 1979 to  
197 December 31, 2013 at Changwu site in Shaanxi, China. The Changwu site is a  
198 transition area between semi-arid and subhumid climate where water limits  
199 agricultural productivity. Monthly averages of all variables were used in this study  
200 because we are mainly interested in seasonal and inter-annual variability.

## 201 **4. Results and discussion**

### 202 **4.1 MWC with orthogonally predictor variables**

203 For the stationary data, there are two narrow horizontal bands (red color)  
204 representing an MWC value of around 1 at the respective scales of 8 and 32 for all  
205 locations (Fig. 2a). These two bands also correspond to the scales of 8 and 32  
206 respectively, for the two predictor variables. When an additional predictor variable  
207 with the scale of 16 is introduced, a wide band from 6 to 40 appears, signifying that  
208 the MWC equals approximately 1 at all locations at the scales of 8, 16, and 32. As  
209 anticipated, when all five predictor variables with scales ranging from 4 to 64 are  
210 included, coherence values of close to 1 are found in the whole scale-location domain



211 (data not shown).

212 The application of MWC to the non-stationary datasets shows that the scales with  
213 significant MWC values gradually increase with the increase in distance. This  
214 increase in the scales is due to the non-stationarity of the variables (Fig. 2b). For  
215 example, when predictor variables of  $z_2$  and  $z_4$  are included, scales of the two bands  
216 corresponding to MWC around 1 increase from 4 to 8 and from 8 to 32, respectively.  
217 Furthermore, as expected, for only one predictor variable (stationary and  
218 non-stationary), MWC reduces to simple wavelet coherence; there is only one band of  
219 coherence around 1, which corresponds to the scale of that predictor variable (data not  
220 shown). Note that the significant MWC values for both stationary and non-stationary  
221 cases are not exactly 1 at all scales or locations due to the smoothing effect along both  
222 scales and locations. However, the mean MWC values of the significant bands are  
223 very high (i.e., 0.94 – 1.00) and the MWC values at the centre of the significant band  
224 are 1, which corresponds to the exact scale of a predictor variable.

225 When the point values in the second half of the data series of a predictor variable is  
226 replaced by 0, the MWC in that half is almost 0 at scales corresponding to that  
227 predictor variable (Fig. 3). For the stationary case, when the point values in the  
228 second half of the data series of predictor variable  $y_2$  (or  $y_4$ ) is replaced by 0, the  
229 MWC is around 1 at the scale of 8 (or 32) in the first half of the transect and 0 in the  
230 second half (Fig. 3a). Similar results were also found for the non-stationary case (Fig.  
231 3b). This is expected because the constant series of 0 is not correlated to the response  
232 variables at any scale. Much like simple wavelet coherence, the MWC method is able



233 to detect abrupt changes in the data series and has the advantages of dealing with  
234 localized multivariate relationships.

#### 235 **4.2 MWC with noised and correlated predictor variables**

236 When  $z_2$  and a noised series derived from  $z_2$  are included as predictor variables,  
237 there is only one band of coherence close to 1 at scales corresponding to  $z_2$ ,  
238 irrespective of the correlation between  $z_2$  and a noised series of  $z_2$  (Fig. 4a). When  $z_2$   
239 and a noised series of  $z_4$  are included as predictor variables, the coherence depends on  
240 the degree of the noise (Fig. 4b). For weakly noised series, there are two bands of  
241 coherence of around 1 corresponding to the scales of  $z_2$  and  $z_4$  respectively. The  
242 PASC is 23%, which equals that of when  $z_2$  and  $z_4$  are included. With the increase of  
243 noise, the coherence and corresponding PASC at the scales corresponding to  $z_4$   
244 decrease. When  $z_2$  and a strongly noised series of  $z_4$  are considered, the band of  
245 coherence around 1 at scales corresponding to  $z_4$  disappears.

246 The inclusion of a third noised  $z_4$  variable substantially increases the area with high  
247 coherence (in red) as compared to the case when only  $z_2$  and  $z_4$  are included (Fig. 4c).  
248 This indicates that MWC will increase with the increase in the number of predictor  
249 variables, with the highest coherence less or equal to 1, irrespective of the number of  
250 predictor variables. However, the area of significant coherence may not necessarily  
251 increase (Ng and Chan, 2012a). In fact, the PASC values for three predictor variables  
252 (19-20%) are lower than for only two predictor variables (23%). This indicates that, in  
253 this case, two predictor variables are better than three in terms of explaining the



254 variations of the response variable. This is because the variance of the response  
255 variable explained by the noised variable is already accounted for by other variables.  
256 Therefore, only an additional variable that can independently explain a fair amount of  
257 variance could contribute significantly to explaining variations of a response variable  
258 (Fig. 4b). This can also explain why there is only one band of coherence around 1 at  
259 scales corresponding to  $z_2$ , when  $z_2$  and a noised series of  $z_2$  are included (Fig. 4a).  
260 This information is helpful in choosing predictor variables for developing  
261 scale-specific predictions, especially when predictor variables are correlated.

#### 262 **4.3 Comparison with other multivariate methods**

##### 263 4.3.1 MSC

264 The MSC as a function of scale is shown in Fig. 5a. For the stationary case, when  
265  $y_2$  and  $y_4$  are included as predictor variables, there are two plateaus centered at the  
266 scales of 8 and 28 representing a coherence of 1. As expected, when an additional  
267 predictor variable  $y_3$  is added, the corresponding scale of 16 also shows coherence of  
268 1. The MSC produces similar scale-specific relationships as MWC does for a  
269 stationary dataset except that the centered scale (i.e., 28) with coherence of 1 deviates  
270 from the expected value (i.e., 32) for predictor variable  $y_4$ . For the non-stationary  
271 case, however, the MSC is much lower than 1 for the predictor variables of  $z_2$  and  $z_4$ ;  
272 MSC of 1 is present only at the scale of 8 when an additional predictor variable  $z_3$  is  
273 added. Obviously, the MSC underestimates the multivariate relationships and is not  
274 suitable to non-stationary processes (Si, 2008) due to its inability to deal with



275 localized features. The MSC at a specific scale provides the average of multivariate  
276 relationships across all locations. Because the scale of a predictor variable changes  
277 with location for the non-stationary case, the MSC deviates greatly from 1.

278 The inability of the MSC to deal with localized features is demonstrated further by  
279 the decrease of MSC at scales when the second half of the included predictor variable  
280 series are replaced by 0 for both the stationary and non-stationary series (Fig. 5b). For  
281 example, when the second half of the  $y_4$  series is replaced by 0 for the stationary case,  
282 the MSC at scales around 32 decreases from 1 to 0.52. Although the MSC can detect  
283 the decrease of coherence at the scales corresponding to the 0 values throughout the  
284 second half of the series, the exact locations for the decrease cannot be identified. In  
285 fact, the coherence decreases only in the second half of the series, and does not  
286 change in the first half of the series. The location for the decrease can be easily  
287 identified by the MWC, but not by MSC.

#### 288 4.3.2 $MCC_{\text{memd}}$

289 Five intrinsic mode functions (IMFs) with non-negligible variance are obtained for  
290 multivariate data series. While the obtained scales for the response variable  $y$  are in  
291 agreement with the true scales for the stationary case, the obtained scales (i.e., 3, 6, 11,  
292 21, and 43) for the response variable  $z$  deviate slightly from the average scales for the  
293 non-stationary case. For the response variable, the contribution of IMFs to the total  
294 variance generally decreases (20% to 13% for stationary and 27% to 11% for  
295 non-stationary) from IMF1 to IMF5, which disagrees with the fact that each scale



296 contributes equally (i.e., 20%) to the total variance. In addition, the sum of variances  
297 over all IMFs for each variable is less than 100% (ranging from 84% to 93%),  
298 indicating that MEMD cannot capture all the variances. For the detailed results of  
299 MEMD, see Supplement, Sect. S5.

300 The  $MCC_{memd}$  as a function of scale is shown in Fig. 6a. For the stationary case,  
301 when predictor variables of  $y_2$  and  $y_4$  are included, the  $MCC_{memd}$  values are 0.98 and  
302 0.93 respectively, at scales corresponding to that of  $y_2$  and  $y_4$ . When a predictor  
303 variable of  $y_3$  is included, the  $MCC_{memd}$  values are 1.00, 1.00, and 0.96 respectively,  
304 at scales corresponding to that of  $y_2$ ,  $y_3$ , and  $y_4$ . For the non-stationary case, the  
305 corresponding  $MCC_{memd}$  values are 0.80 and 0.85 for the two predictor variable case,  
306 and 0.95, 0.99, and 0.91 respectively, for the case of three predictor variables.  
307 Therefore, the  $MCC_{memd}$  can be used to determine the scale-specific multivariate  
308 relationships. Similar to MSC, however, the  $MCC_{memd}$  underestimates the multivariate  
309 relationships, especially for the non-stationary case with less predictor variables. On  
310 the contrary, the  $MCC_{memd}$  can also overestimate the multivariate relationships. For  
311 example, when only predictor variables corresponding to scales of 8, 16, and 32 are  
312 considered, the  $MCC_{memd}$  value for the stationary case is 0.47 at the scale of 64, which  
313 deviates much from the expected  $MCC_{memd}$  value of 0 (Fig. 6a). The possible  
314 underestimation and overestimation by the  $MCC_{memd}$  may come from the  
315 decomposition errors inherent in the MEMD algorithm (Rehman and Mandic, 2010).

316 Similar to MSC, the localized multivariate relationships cannot be obtained from  
317  $MCC_{memd}$ . This can be better explained by the decrease of  $MCC_{memd}$  when half of the



318 series of the predictor variables are replaced by 0 (Fig. 6b). For the stationary case,  
319 the  $MCC_{memd}$  values at the scales corresponding to y2 (or y4) decrease from 0.98 to  
320 0.49 and from 0.93 to 0.62 when the second half of the y2 (or y4) series are replaced  
321 by 0.

322 As explained above, the MWC has advantages in untangling localized multivariate  
323 relationships as compared to the common multivariate methods. It is important to  
324 reveal the multivariate relationships, which vary with time or space that are associated  
325 with different processes. For example, discharge usually happens on knolls, while  
326 recharge usually happens in neighboring depressions (Gates et al., 2011). Therefore,  
327 the controlling factors of soil water storage may vary with the land element  
328 characteristics of a location. For example, local controls may be more important on  
329 knolls, while non-local controls may be more important in depressions (Grayson et al.,  
330 1997). In a temporal domain, vegetation transpiration contributes more to the  
331 evapotranspiration in the growing seasons, which may result in the changes of  
332 environmental factors explaining temporal variations of evapotranspiration in  
333 different seasons.

#### 334 **4.4 Application of the MWC**

335 Each meteorological factor was significantly correlated to the  $E$ , but the dominant  
336 factors explaining variation in  $E$  differed with scale. For example, the relative  
337 humidity was the dominating factor at small (2–8 months) and large (>32 months)  
338 scales, while temperature was the dominating factor at the medium (8–32 months)





339 scales. Overall, the relative humidity corresponded to the greatest mean MWC (0.62)  
340 and PASC value (40%) at multiple scale-location domains. For the detailed  
341 relationships between  $E$  and each factor, see Supplement, Sect. S6.

342 The MWC analysis shows that the combination of relative humidity and mean  
343 temperature produced the greatest mean MWC (0.82) and PASC (49%) among all  
344 two-factor cases, indicating that they are the best to explain variations in  $E$  at multiple  
345 scale-location domains (Fig. 7a). However, adding an additional factor such as sun  
346 hours, which was the best among all three-factor cases, increased the average  
347 coherence (0.91), but slightly decreased the PASC to 48% (Fig. 7b). This indicated  
348 that sun hours was not significantly different from red noise in explaining additional  
349 variation in  $E$ . Similar results were found when the wind speed was added. The reason  
350 for this was that most areas with significant coherence between  $E$  and sun hours or  
351 wind speed, were a subset of areas with significant coherence between  $E$  and relative  
352 humidity or mean temperature (see Supplement, Sect. S3). Therefore, relative  
353 humidity and mean temperature were adequate to explain the temporal variation of  $E$   
354 at various scales at this site. This is consistent with Li et al. (2012), who indicate that  
355 relative humidity and mean temperature are the two main contributors to the temporal  
356 change of potential evapotranspiration on the Chinese Loess Plateau.

## 357 5. Conclusions

358 Multiple wavelet coherence is developed to determine scale-specific and localized  
359 multivariate relationships in geosciences. The new method is tested and compared



360 with existing multivariate methods using an artificial dataset. The new method can be  
361 used to determine the proportion of the variance of a response variable that is  
362 explained by predictor variables at a specific scale and location (spatially or  
363 temporally). As compared with simple wavelet coherence, more variation may be  
364 explained at multiple scale-location domains by the MWC. Including more variables  
365 is only beneficial if the variables are not strongly cross-correlated and can  
366 independently explain a fair amount of variability in a response variable. Therefore,  
367 the best combinations of variables that explain multivariate spatial or temporal  
368 variability at multiple scales can be determined. This is important for optimizing  
369 variables for developing scale-specific prediction. The MSC and  $MCC_{memd}$  can  
370 determine multivariate relationships at multiple scales, but localized multivariate  
371 relationships are not available and both MSC and  $MCC_{memd}$  are likely to  
372 underestimate the degree of multivariate relationships for non-stationary processes. In  
373 addition, the performance of  $MCC_{memd}$  relies on the performance of MEMD, which  
374 needs further development. Application of the MWC into the real dataset indicates  
375 that the combination of relative humidity and mean temperature are the optimal  
376 factors to explain temporal variation of  $E$  at the Changwu site in China.

377 In summary, multiple wavelet coherence has advantages over existing multivariate  
378 methods, and provides an effective vehicle for untangling complex spatial or temporal  
379 variability for multiple controlling factors at multiple scales and locations. It may also  
380 be used as a data-driven tool for modeling and predicting various processes in the area  
381 of geosciences such as precipitation, drought, soil water dynamics, stream flow, and



382 atmospheric circulation.

### 383 **Acknowledgements**

384 The Matlab codes for calculating multiple wavelet coherence are developed based on  
385 the codes provided by A. Grinsted  
386 (<http://noc.ac.uk/using-science/crosswavelet-wavelet-coherence>) and, together with  
387 user manual, are available in the Supplement (Sect. S2-S4). The project was partially  
388 funded by the Natural Sciences and Engineering Research Council of Canada  
389 (NSERC) and Agriculture Development Fund of Saskatchewan.

### 390 **References**

391 Biswas, A. and Si, B. C.: Identifying scale specific controls of soil water storage in a  
392 hummocky landscape using wavelet coherency, *Geoderma*, 165, 50–59, doi:  
393 10.1016/j.geoderma.2011.07.002, 2011.

394 Carey, S. K., Tetzlaff, D., Buttle, J., Laudon, H., McDonnell, J., McGuire, K., Seibert,  
395 J., Soulsby, C., and Shanley, J.: Use of color maps and wavelet coherence to discern  
396 seasonal and interannual climate influences on streamflow variability in northern  
397 catchments, *Water Resour. Res.*, 49, 6194–6207, doi: 10.1002/wrcr.20469, 2013.

398 Das, N.N. and Mohanty, B. P.: Temporal dynamics of PSR-based soil moisture across  
399 spatial scales in an agricultural landscape during SMEX02: A wavelet approach,  
400 *Remote Sens. Environ.*, 112, 522–534, doi:10.1016/j.rse.2007.05.007, 2008.

401 Gates, J. B., Scanlon, B. R., Mu, X. M., and Zhang, L.: Impacts of soil conservation



402 on groundwater recharge in the semi-arid Loess Plateau, China, *Hydrogeol. J.*, 19,  
403 865–875, 2011.

404 Graf, A., Bogena, H. R., Drüe, C., Hardelauf, H., Pütz, T., Heinemann, G., and  
405 Vereecken, H.: Spatiotemporal relations between water budget components and soil  
406 water content in a forested tributary catchment, *Water Resour. Res.*, 50, 4837–4857,  
407 doi:10.1002/2013WR014516, 2014.

408 Grayson, R. B., Western, A. W., Chiew, F. H. S., and Blöschl, G.: Preferred states in  
409 spatial soil moisture patterns: local and nonlocal controls, *Water Resour. Res.*, 33,  
410 2897–2908, doi: 10.1029/97WR02174, 1997.

411 Grinsted, A., Moore, J. C., and Jevrejeva, S.: Application of the cross wavelet  
412 transform and wavelet coherence to geophysical time series, *Nonlinear Proc. Geoph.*,  
413 11, 561–566, 2004.

414 Hu, W., Biswas, A., and Si, B. C.: Application of multivariate empirical mode  
415 decomposition for revealing scale- and season-specific time stability of soil water  
416 storage, *Catena*, 113, 377–385, doi:10.1016/j.catena.2013.08.024, 2014.

417 Hu, W. and Si, B. C.: Soil water prediction based on its scale-specific control using  
418 multivariate empirical mode decomposition, *Geoderma*, 193–194, 180–188, doi:  
419 10.1016/j.geoderma.2012.10.021, 2013.

420 Koopmans, L. H.: *The spectral analysis of time series*, Academic Press, New York,  
421 1974.

422 Labat, D.: Recent advances in wavelet analyses: Part I. A review of concepts, *J.*  
423 *Hydrol.*, 314, 275–288, doi: 10.1016/j.jhydrol.2005.04.003, 2005.



- 424 Lakshmi, V., Piechota, T., Narayan, U., and Tang, C. L.: Soil moisture as an indicator  
425 of weather extremes, *Geophys. Res. Lett.*, 31, L11401, doi:10.1029/2004GL019930,  
426 2004.
- 427 Li, Z., Zheng, F. L., and Liu, W. Z.: Spatiotemporal characteristics of reference  
428 evapotranspiration during 1961–2009 and its projected changes during 2011–2099 on  
429 the Loess Plateau of China, *Agric. For. Meteorol.*, 154–155, 147–155,  
430 doi:10.1016/j.agrformet.2011.10.019, 2012.
- 431 Mihanović, H., Qrlić, M., and Pasrić, Z.: Diurnal thermocline oscillations driven by  
432 tidal flow around an island in the Middle Adriatic, *J. Marine Syst.*, 78, S157–S168,  
433 doi: 10.1016/j.jmarsys.2009.01.021, 2009.
- 434 Müller, W. A., Frankignoul, C., and Chouaib, N.: Observed decadal tropical  
435 Pacific–North Atlantic teleconnections, *Geophys. Res. Lett.*, 35, L24810,  
436 doi:10.1029/2008GL035901, 2008.
- 437 Ng, E. K. W. and Chan, J. C. L.: Geophysical applications of partial wavelet  
438 coherence and multiple wavelet coherence, *J. Atmos. Ocean. Tech.*, 29, 1845–1853,  
439 doi: 10.1175/JTECH-D-12-00056.1, 2012a.
- 440 Ng, E. K. W. and Chan, J. C. L.: Interannual variations of tropical cyclone activity  
441 over the north Indian Ocean, *Int. J. Climatol.*, 32, 819–830, doi: 10.1002/joc.2304,  
442 2012b.
- 443 Polansky, L., Wittemyer, G., Cross, P. C., Tambling, C. J., and Getz, W. M.: From  
444 moonlight to movement and synchronized randomness: Fourier and wavelet analyses  
445 of animal location time series data, *Ecology*, 91, 1506–1518, doi: 10.1890/08-2159.1,



- 446 2010.
- 447 Rehman, N. and Mandic, D. P.: Multivariate empirical mode decomposition, Proc. R.
- 448 Soc. A., 466, 1291–1302, doi:10.1098/rspa.2009.0502, 2010.
- 449 She, D. L., Liu, D. D., Peng, S. Z., and Shao, M. A.: Multiscale influences of soil
- 450 properties on soil water content distribution in a watershed on the Chinese Loess
- 451 Plateau, Soil Sci., 178, 530–539, doi: 10.1097/SS.000000000000021, 2013.
- 452 She, D. L., Zheng, J. X., Shao, M. A., Timm, L. C., and Xia, Y. Q.: Multivariate
- 453 empirical mode decomposition derived multi-scale spatial relationships between
- 454 saturated hydraulic conductivity and basic soil properties, Clean-Soil Air Water, doi:
- 455 10.1002/clen.201400143, 2015.
- 456 Si, B. C.: Spatial scaling analyses of soil physical properties: A review of spectral and
- 457 wavelet methods, Vadose Zone J., 7, 547–562, doi: 10.2136/vzj2007.0040, 2008.
- 458 Si, B. C. and Zeleke, T. B.: Wavelet coherency analysis to relate saturated hydraulic
- 459 properties to soil physical properties, Water Resour. Res., 41, W11424,
- 460 doi:10.1029/2005WR004118, 2005.
- 461 Tang, C. L. and Piechota, T. C.: Spatial and temporal soil moisture and drought
- 462 variability in the Upper Colorado River Basin, J. Hydrol., 379, 122–135, doi:
- 463 10.1016/j.jhydrol.2009.09.052, 2009.
- 464 Torrence, C. and Compo, G. P.: A practical guide to wavelet analysis, Bull. Am.
- 465 Meteorol. Soc., 79, 61–78, doi: 10.1175/1520-0477(1998)079<0061:apgtwa>2.0.co;2,
- 466 1998.
- 467 Torrence, C. and Webster, P. J.: Interdecadal changes in the ENSO-monsoon system, J.



468 Clim., 12, 2679–2690, doi: 10.1175/1520-0442(1999)012<2679:ICITEM>2.0.CO;2,

469 1999.

470 Yan, R. and Gao, R. X.: A tour of the Hilbert–Huang transform: an empirical tool for

471 signal analysis, IEEE Instrum. Meas. Mag., 10, 40–45, doi:

472 10.1109/MIM.2007.4343566, 2007.



473 **Figure captions**

474 **Figure 1.** (a) Stationary and (b) non-stationary series of response variables (y for  
475 stationary and z for non-stationary case) encompassing five cosine waves (y1 to y5  
476 for stationary and z1 to z5 for non-stationary case) with different dimensionless  
477 scales.

478 **Figure 2.** Multiple wavelet coherence (a) between response variable y and predictor  
479 variables y2 and y4; (b) between response y and predictors y2, y3, and y4; (c)  
480 between response z and predictors z2 and z4; and (d) between response z and  
481 predictors z2, z3, and z4. The artificial data series (y) encompasses five cosine waves  
482 (y1, y2, y3, y4, and y5) with different scales for the stationary case, and the artificial  
483 data series (z) encompasses five cosine waves (z1, z2, z3, z4, and z5) with different  
484 scales for the non-stationary case. The predictor variables, connected by a hyphen, are  
485 shown in the top right corner of each subplot. Thin solid lines demarcate the cones of  
486 influence, and thick solid lines show the 95% confidence levels.

487 **Figure 3.** Multiple wavelet coherence (a) between y and y2h0 and y4; (b) between y  
488 and y2 and y4h0; (c) between z and z2h0 and z4; and (d) between z and z2 and z4h0.  
489 The artificial data series (y) encompasses five cosine waves (y1, y2, y3, y4, and y5)  
490 with different scales for the stationary case and the artificial data series (z)  
491 encompasses five cosine waves (z1, z2, z3, z4, and z5) with different scales for the  
492 non-stationary case. The variables y2h0 (or z2h0) and y4h0 (or z4h0) refer to the new  
493 series of y2 (or z2) and y4 (or z4), in which the second half is replaced by 0. The





494 predictor variables, connected by a hyphen, are shown in the top right corner of each  
495 subplot. Thin solid lines demarcate the cones of influence and thick solid lines show  
496 the 95% confidence levels.

497 **Figure 4.** Multiple wavelet coherence of an artificial data series ( $z$ ) encompassing five  
498 cosine waves ( $z_1, z_2, z_3, z_4,$  and  $z_5$ ) with different scales and (a)  $z_2$  and noised  $z_2$ , (b)  
499  $z_2$  and noised  $z_4$ , and (c)  $z_2, z_4,$  and noised  $z_4$  for the non-stationary case. The  
500 predictor variables are connected by a hyphen and shown in the top right corner of  
501 each subplot.  $z_2wn$  ( $z_4wn$ ),  $z_2mn$  ( $z_4mn$ ), and  $z_2sn$  ( $z_4sn$ ) indicate weakly,  
502 moderately, and strongly noised  $z_2$  ( $z_4$ ) series respectively. Weakly, moderately, and  
503 strongly noised series are correlated with original series, having correlation  
504 coefficients of 0.9, 0.5, and 0.1 respectively. Thin solid lines demarcate the cones of  
505 influence and thick solid lines show the 95% confidence levels.

506 **Figure 5.** Multiple spectral coherence (MSC) of an artificial data series ( $y$  or  $z$ )  
507 encompassing five cosine waves ( $y_1$  to  $y_5$ ; or  $z_1$  to  $z_5$ ) with different scales and (a)  
508 two ( $y_2$  and  $y_4$ ; or  $z_2$  and  $z_4$ ) or three ( $y_2, y_3,$  and  $y_4$ ; or  $z_2, z_3,$  and  $z_4$ ) data series,  
509 and (b) two ( $y_2$  and  $y_4$ ; or  $z_2$  and  $z_4$ ) data series when the second half of one data  
510 series is replaced by 0. The variables  $y_2h0$  (or  $z_2h0$ ) and  $y_4h0$  (or  $z_4h0$ ) refer to the  
511 new series of  $y_2$  (or  $z_2$ ) and  $y_4$  (or  $z_4$ ) in which the second half is replaced by 0.

512 **Figure 6.** Multiple correlation coefficient between multivariate empirical mode  
513 decomposition ( $MCC_{memd}$ ) of an artificial series ( $y$  or  $z$ ) and (a) two ( $y_2$  and  $y_4$ ; or  $z_2$   
514 and  $z_4$ ) or three ( $y_2, y_3,$  and  $y_4$ ; or  $z_2, z_3,$  and  $z_4$ ) data series, and (b) two ( $y_2$  and  $y_4$ ;  
515 or  $z_2$  and  $z_4$ ) data series when the second half of one data series is replaced by 0. The



516 variables  $y_{2h0}$  (or  $z_{2h0}$ ) and  $y_{4h0}$  (or  $z_{4h0}$ ) refer to the new series of  $y_2$  (or  $z_2$ ) and  
517  $y_4$  (or  $z_4$ ) in which the second half is replaced by 0.

518 **Figure 7.** Multiple wavelet coherence between evaporation ( $E$ ) from water surfaces  
519 and meteorological factors ((a) relative humidity and mean temperature and (b)  
520 relative humidity, mean temperature, and sun hours) at Changwu site in Shaanxi,  
521 China. Thin solid lines demarcate the cones of influence, and thick solid lines show  
522 the 95% confidence level.

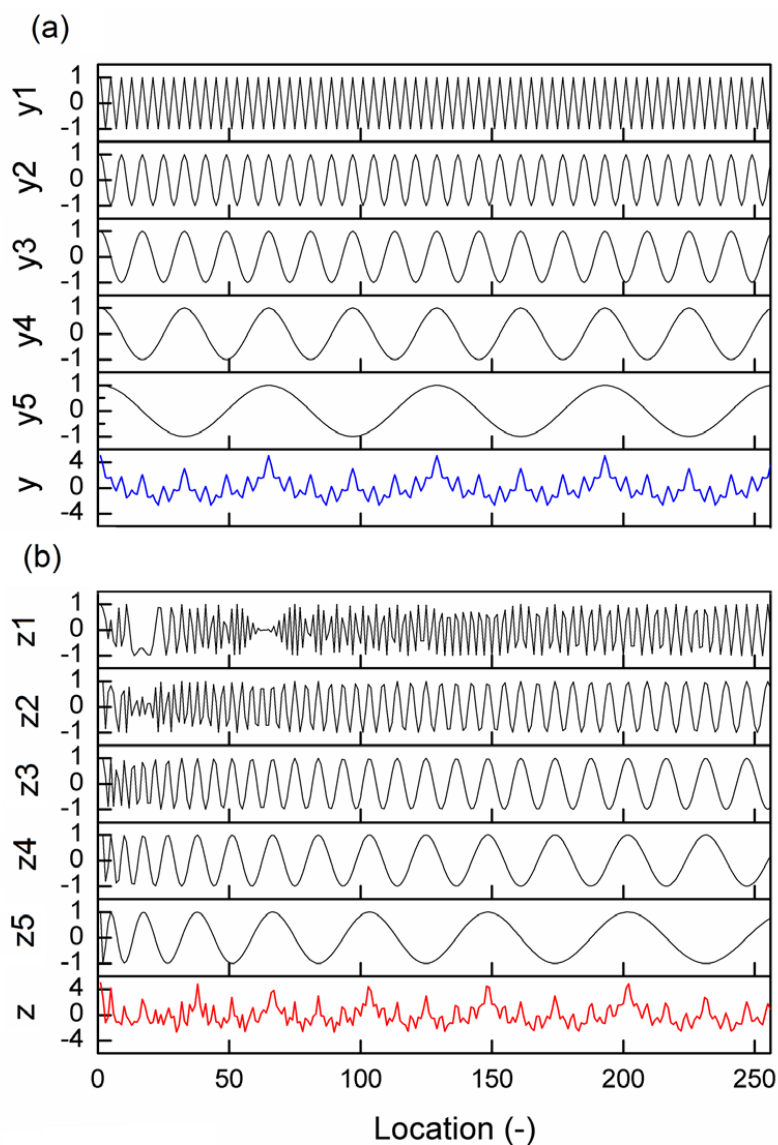


**Figure 1.** (a) Stationary and (b) non-stationary series of response variables ( $y$  for stationary and  $z$  for non-stationary case) encompassing five cosine waves ( $y1$  to  $y5$  for stationary and  $z1$  to  $z5$  for non-stationary case) with different dimensionless scales.

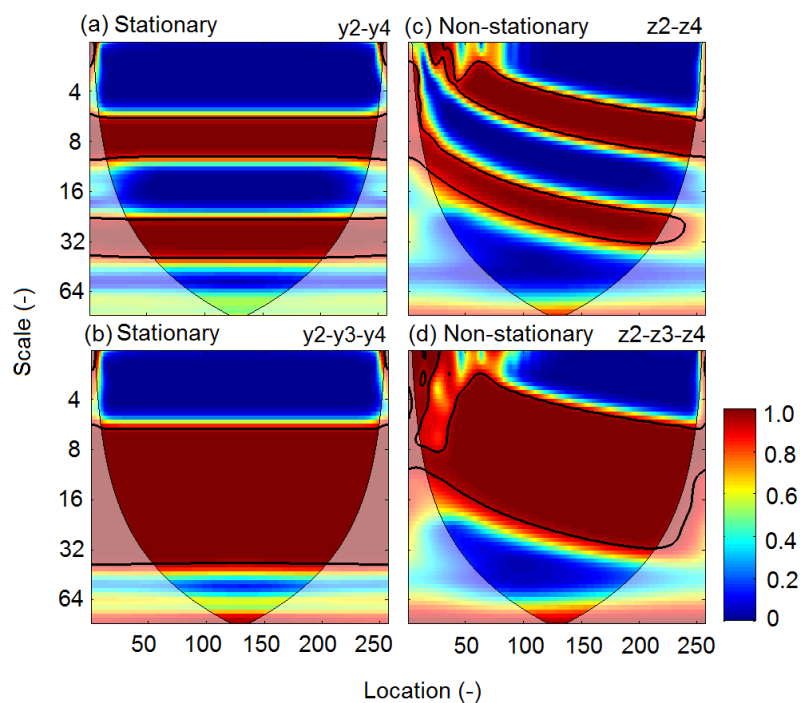


**Figure 2.** Multiple wavelet coherence (a) between response variable  $y$  and predictor variables  $y_2$  and  $y_4$ ; (b) between response  $y$  and predictors  $y_2$ ,  $y_3$ , and  $y_4$ ; (c) between response  $z$  and predictors  $z_2$  and  $z_4$ ; and (d) between response  $z$  and predictors  $z_2$ ,  $z_3$ , and  $z_4$ . The artificial data series ( $y$ ) encompasses five cosine waves ( $y_1$ ,  $y_2$ ,  $y_3$ ,  $y_4$ , and  $y_5$ ) with different scales for the stationary case, and the artificial data series ( $z$ ) encompasses five cosine waves ( $z_1$ ,  $z_2$ ,  $z_3$ ,  $z_4$ , and  $z_5$ ) with different scales for the non-stationary case. The predictor variables, connected by a hyphen, are shown in the top right corner of each subplot. Thin solid lines demarcate the cones of influence, and thick solid lines show the 95% confidence levels.

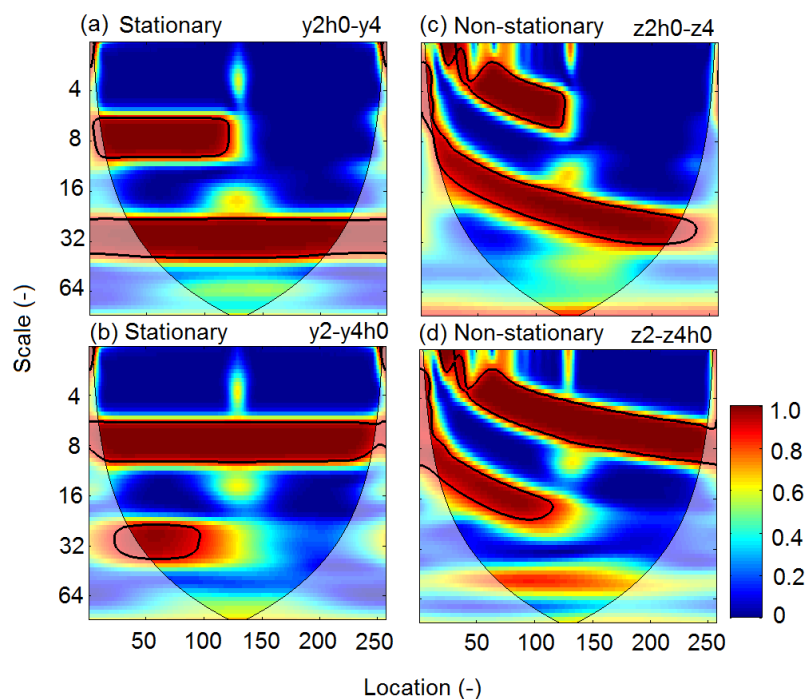


**Figure 3.** Multiple wavelet coherence (a) between  $y$  and  $y2h0$  and  $y4$ ; (b) between  $y$  and  $y2$  and  $y4h0$ ; (c) between  $z$  and  $z2h0$  and  $z4$ ; and (d) between  $z$  and  $z2$  and  $z4h0$ . The artificial data series ( $y$ ) encompasses five cosine waves ( $y1$ ,  $y2$ ,  $y3$ ,  $y4$ , and  $y5$ ) with different scales for the stationary case and the artificial data series ( $z$ ) encompasses five cosine waves ( $z1$ ,  $z2$ ,  $z3$ ,  $z4$ , and  $z5$ ) with different scales for the non-stationary case. The variables  $y2h0$  (or  $z2h0$ ) and  $y4h0$  (or  $z4h0$ ) refer to the new series of  $y2$  (or  $z2$ ) and  $y4$  (or  $z4$ ), in which the second half is replaced by 0. The predictor variables, connected by a hyphen, are shown in the top right corner of each subplot. Thin solid lines demarcate the cones of influence and thick solid lines show the 95% confidence levels.

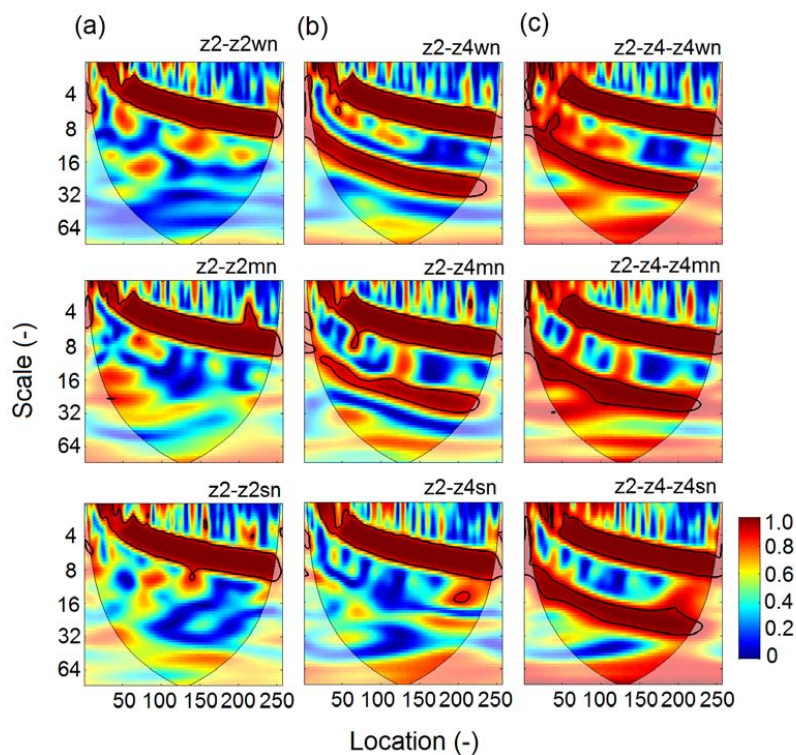


**Figure 4.** Multiple wavelet coherence of an artificial data series ( $z$ ) encompassing five cosine waves ( $z_1$ ,  $z_2$ ,  $z_3$ ,  $z_4$ , and  $z_5$ ) with different scales and (a)  $z_2$  and noised  $z_2$ , (b)  $z_2$  and noised  $z_4$ , and (c)  $z_2$ ,  $z_4$ , and noised  $z_4$  for the non-stationary case. The predictor variables are connected by a hyphen and shown in the top right corner of each subplot.  $z_2wn$  ( $z_4wn$ ),  $z_2mn$  ( $z_4mn$ ), and  $z_2sn$  ( $z_4sn$ ) indicate weakly, moderately, and strongly noised  $z_2$  ( $z_4$ ) series, respectively. Weakly, moderately, and strongly noised series are correlated with original series, having with correlation coefficients of 0.9, 0.5, and 0.1, respectively. Thin solid lines demarcate the cones of influence and thick solid lines show the 95% confidence levels.

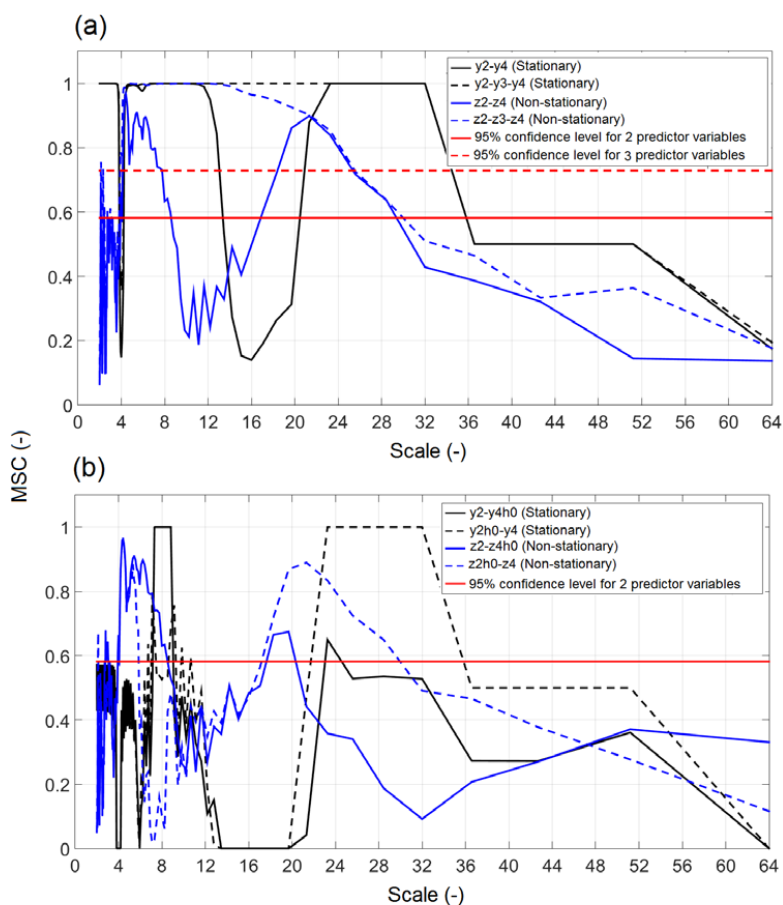


**Figure 5.** Multiple spectral coherence (MSC) of an artificial data series (y or z) encompassing five cosine waves (y1 to y5; or z1 to z5) with different scales and (a) two (y2 and y4; or z2 and z4) or three (y2, y3, and y4; or z2, z3, and z4) data series, and (b) two (y2 and y4; or z2 and z4) data series when the second half of one data series is replaced by 0. The variables y2h0 (or z2h0) and y4h0 (or z4h0) refer to the new series of y2 (or z2) and y4 (or z4) in which the second half is replaced by 0.

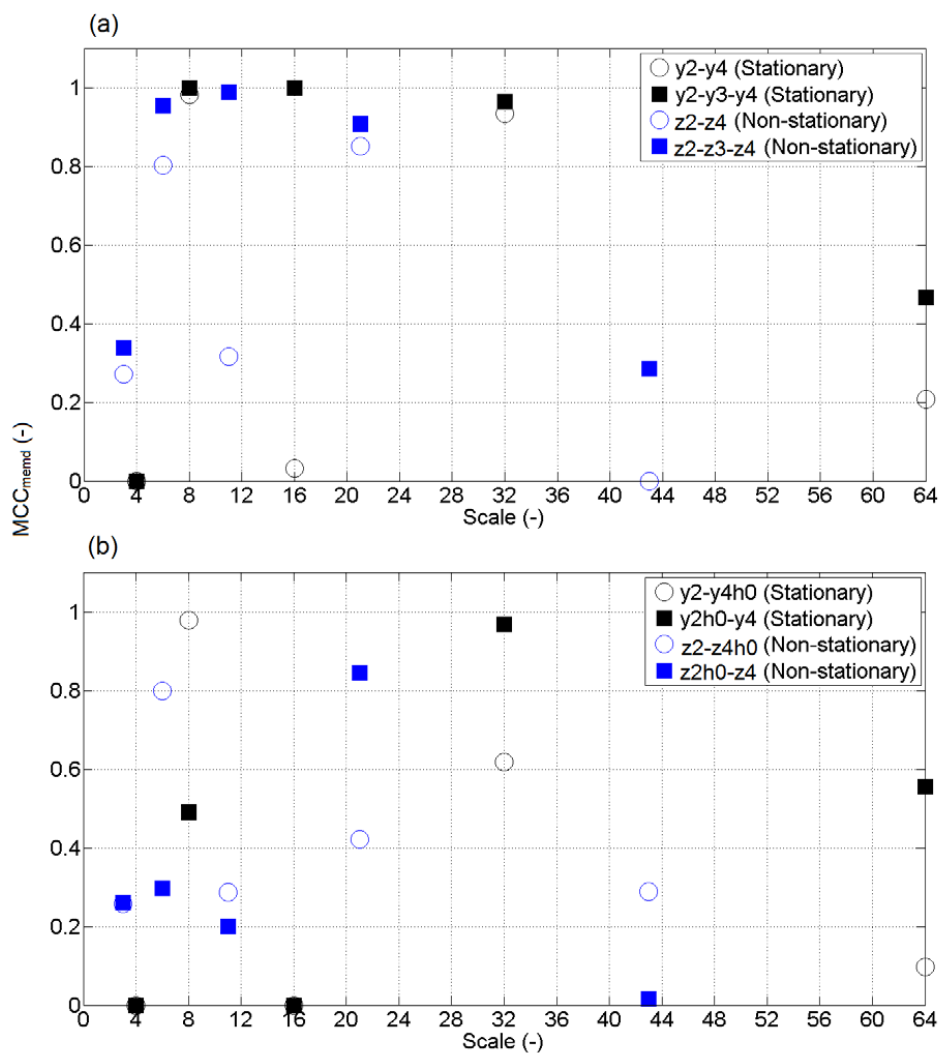


**Figure 6.** Multiple correlation coefficient between multivariate empirical mode decomposition ( $MCC_{memd}$ ) of an artificial series ( $y$  or  $z$ ) and (a) two ( $y2$  and  $y4$ ; or  $z2$  and  $z4$ ) or three ( $y2$ ,  $y3$ , and  $y4$ ; or  $z2$ ,  $z3$ , and  $z4$ ) data series, and (b) two ( $y2$  and  $y4$ ; or  $z2$  and  $z4$ ) data series when the second half of one data series is replaced by 0. The variables  $y2h0$  (or  $z2h0$ ) and  $y4h0$  (or  $z4h0$ ) refer to the new series of  $y2$  (or  $z2$ ) and  $y4$  (or  $z4$ ) in which the second half is replaced by 0.



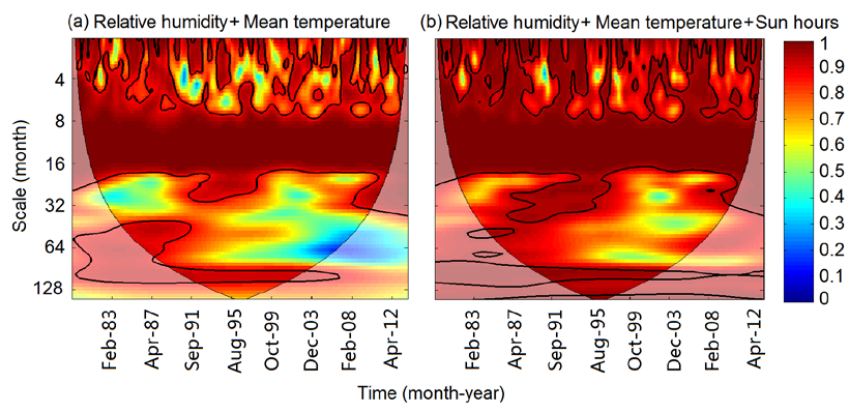


**Figure 7.** Multiple wavelet coherence between evaporation (E) from water surfaces and meteorological factors ((a) relative humidity and mean temperature and, (b) relative humidity, mean temperature, and sun hours) at Changwu site in Shaanxi, China. Thin solid lines demarcate the cones of influence, and thick solid lines show the 95% confidence level.